ICAS 2020 SHANG HAI
International Council of the Aeronautical Sciences
32nd Congress of the International Council of the Aeronautical Sciences
September 6-10, 2021
Pudong Shangri-La, Shanghai, China

TOTAL TEMPERATURE MEASUREMENTS IN WATER INJECTION AND PRE-COMPRESSOR COOLING TECHNOLOGY

Geng Xin, Liu Xupeng, Song Zhenyu, Zhang Long

AECC Shenyang Engine Research Institute, Shenyang 110015, China

Abstract

Water Injection Pre-Compressor Cooling (WIPCC) technique is an effective way to achieve high Mach number flight. While the air temperature can hardly be measured due to contamination of droplets. To solve this problem, a probe rake with corresponding calibration and test method is proposed. Different from conventional test, the measuring point of probe rake is backward to the airflow to separate the droplets. To obtain the forward total temperature, a calibration procedure is proposed which establishes the correlation between the forward and backward temperature. A computational fluid dynamic model (CFD) of the flow is also conducted to get a deep understanding. Comparison of simulation results with experimental data show good predicted trends.

Keywords: Water Injection Pre-Compressor Cooling; contamination of droplets; temperature probe; water-air loading ratio;

1. Introduction

In recent years, high-speed aircraft has become a key research direction in the aviation field, and WIPCC technology has received more and more attentions as one of the convenient and economic key power technologies. This technology sprays an appropriate amount of cooling water in front of the compressor inlet to reduce the airflow temperature, thereby increasing the mass flow rate. At the same time, the injected liquid water vaporizes, which could also increase the thrust of the engine. Since Wilcox [1] proposed the theory of WIPCC technology in 1951, a large number of relevant studies have been carried out. Meher [2] conducted a large number of experiments and theoretical studies on this technology from the perspective of combined gas turbine design. Daniel [3] conducted a research of gas emissions and engine thrust on small pressure ratios engines. Shang Xusheng [4] established a mathematical model considering variable specific heat to calculate engine performance according to the working mechanism of the technology. In addition to researches on the design of combined gas turbines, researches on water spray atomization technology have also been carried out. Sanaye [5], Zhang Hai [6] and Tu Hongyan [7] respectively adopted computational fluid dynamics ways to study the evaporation of spray water, cooling of air flow, and pressure reduction of pipelines. Chaker [8] carried out research on water spray atomization, water droplet motion and nozzle design from the experimental and theoretical aspects. The research mentioned above theoretically analyzed the changes of aerodynamic parameters after spray, but there is little measurement research, especially temperature measurement. Using conventional temperature measurement methods, the measuring point of the probe will be contaminated by droplets, leading to an invalid result. In regard to this, Stickney [9] designed a Rosemount centrifugal temperature probe. The fairing of the probe contains two flow paths, which are approximately vertical, and use inertia to separate water and gas; Willems [10] designed a temperature probe for large-scale steam turbine experiments, and designed multiple partitions in the cavity to separate water and gas. The common feature of the above two types of temperature probes is that the water vapor is separated inside the probe, which needs a large volume. It is suitable for single-point temperature measurement, but it is difficult to meet the actual requirements of aero-engine radial multi-point temperature test.
For this reason, a probe rake is designed in this paper to perform multi-point temperature testing on

the radial direction of the flow field in a water spray environment. The performance is verified on the WIPCC test bench, and the test results are compared with the numerical simulation results.

2. Test and methods

2.1 Test bench and probe rake

The experimental test, as shown in Figure 1, is carried out in a high temperature tunnel with a diameter of 300 mm and a thickness of 10mm. The heating test verifies that the tunnel can be considered adiabatic. The nozzles are evenly distributed on the jet spray rod to realize cooling the heated gas by spraying water droplets with mean diameter of 50μm. Three sections were chosen to measure the temperature after the rod at the distance of 3D,5.5D and 8D (D denotes the diameter of the section), respectively.

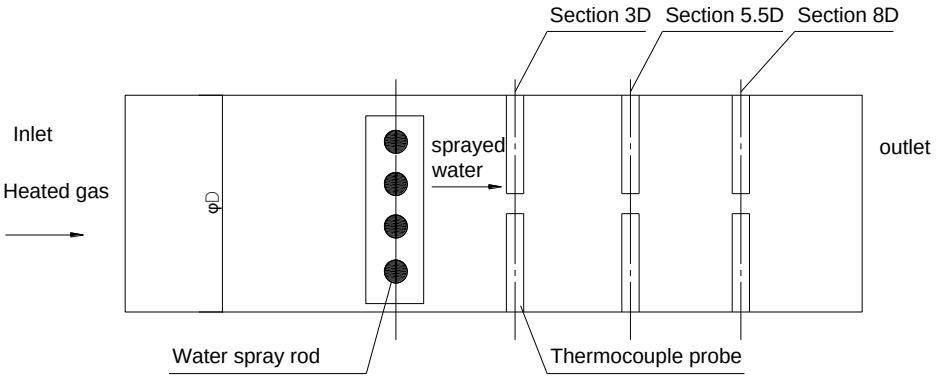

Figure 1 - Schematic diagram of WIPCC test bench

The probe combines a conventional probe rake with a new designed circular arc protective cover to reduce the water hit on the probe strut. The probe rake has three measuring point at 0.4R, 0.7R, 0.9R distance from the axis of the tunnel, respectively.

2.2 Calibration and test method

A reversed test method is proposed which means that the probe is fixed with measuring point backward to the airflow to separate the water droplets. The inertia of the water droplet is much larger than the air, so the droplets trajectory remains unchanged while the airflow does not. As shown in Figure 2, due to the impact of the droplets, one part of the water impacts the protective cover, causing adsorption and splashing, while the other part maintains original motion without contacting the measuring point. Unlike the droplet, airflow can bypass the protective cover to flush the measuring point. Thus, a water droplet masking zone is formed at the measuring point to obtain the pure air temperature.

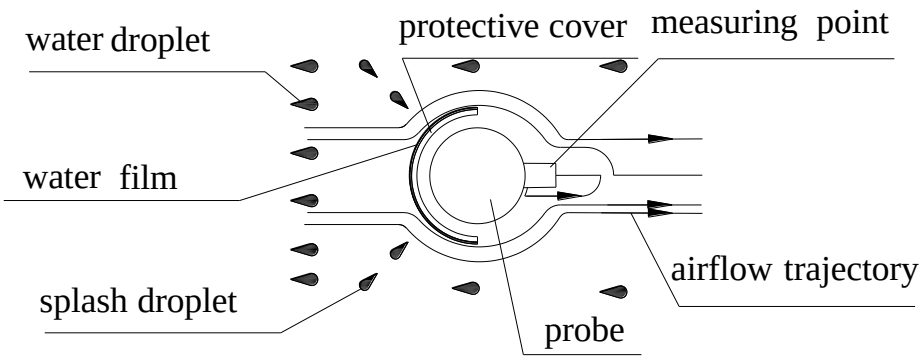

Figure 2 - Schematic diagram of reversed test principle

The reversed test result is not the total temperature of the air and therefore a corresponding on-site

calibration procedure is presented. Assuming that the measuring point can get rid of the water spray in the reversed test, and the heat conduction can be ignored if good insulation is provided, the calibration results will be same as no water sprayed case. Then the temperature correlation between the forward and backward measuring point can be established. For example, four probes each with three measuring points were used in the test. Firstly, they were faced forward the airflow as shown in Figure 3(a) and equally spaced temperature gradients were selected within the test temperature range as references to heat the flow. The four probes were marked as T1-T4 clockwise. Secondly, T1 and T3 remained stationary, as shown in Figure 3(b) while T2 and T4 were faced backward the airflow to perform the same temperature gradients test of the first step. Then, as shown in Figure 4 the average temperature of T1 and T3 was plotted on the abscissa, and the average temperature of T2 and T4 was plotted on the ordinate to establish a fitting formula. Two linear fits ($y_1 = f(x)$ and $y_2 = g(x)$) could be obtained with very high correlation coefficients (R^2 value), equal to or higher than 0.9998 in this case. Finally, a correlation formula which illustrated the forward temperature and the backward temperature could be derived as $y_1 = \varphi(y_2)$.

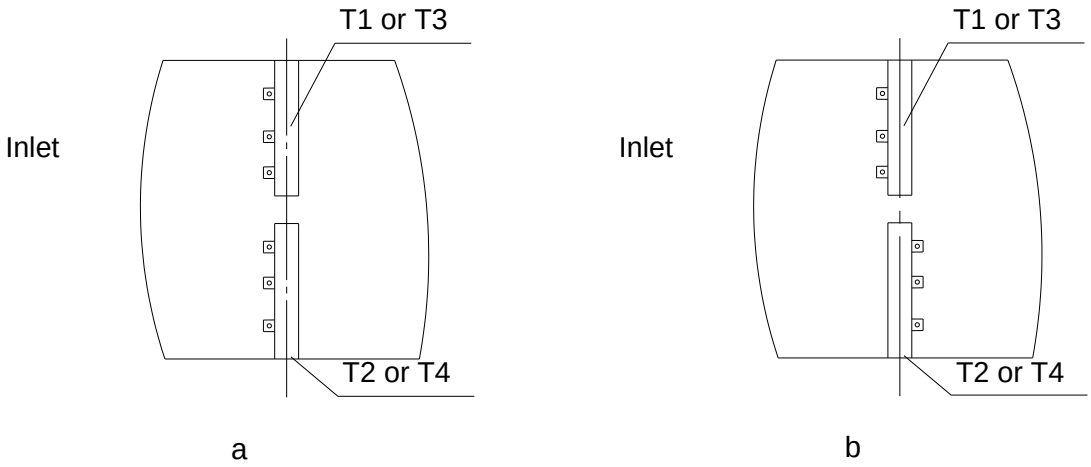

Figure 3 - Assembly diagram of forward and backward calibration method

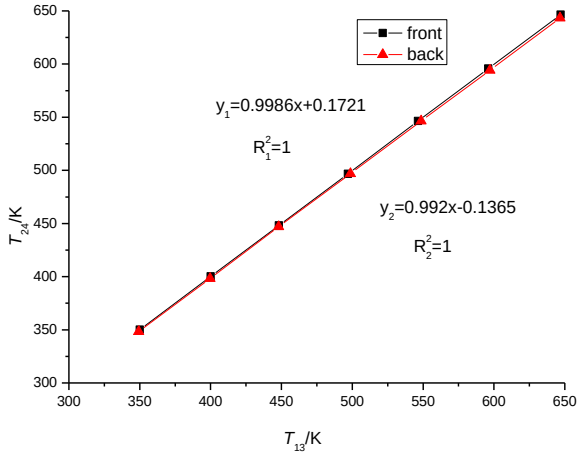

Figure 4 - Calibration curve

3. Experiments and CFD simulations

The inlet air flow was kept at the rate of 4.87kg/s with the total pressure of 1.25×10^5 Pa and Mach number of 0.23. The measurement was carried out at 2%, 3%, 4%, 5%, and 5.5% of the water-air loading ratio. In each state, the gas was heated to 616K steadily, then water was sprayed at target

water-air loading ratio. The experiment was repeated three times to rule out accidental results.
For the simplicity and accuracy of the simulation results, the two-phase flow in the test bench is modeled without the probe. The simulation is conducted by ANSYS Fluent software's realizable k-ε turbulence model. The gas is set as ideal air with viscosity following Sutherland's law in the Euler coordinate system. The water droplet is set as a discrete phase, calculated in the Lagrange coordinate system. The two-way coupling effect of the water droplet and gas is also considered.
The gas continuous equation is defined as

$$\frac{\partial \rho_g}{\partial t} + \nabla \cdot \left(\rho_g u_g\right) = 0 \tag{1}$$

where ρ_g is the density of air, u_g is the gas velocity.
The momentum equation of gas is expressed as

$$\frac{\partial \rho_g u_g}{\partial t} + \nabla \cdot \left(\rho_g u_g u_g\right) = -\frac{\partial p}{\partial x} + \rho_g g + \nabla \cdot \tau_g + F \tag{2}$$

on which p refers to static pressure and F means external volume force. In addition, stress tensor term τ_g is given by

$$\tau_g = \mu\left(\frac{\partial u_i}{\partial x_j} + \frac{\partial u_j}{\partial x_i} - \frac{2}{3}\frac{\partial u_l}{\partial x_l}\delta\right) \tag{3}$$

The dynamic viscosity μ is determined by Sutherland's law. The subscript of u and x represent the component of velocity and coordinate system.
The energy equation of the gas is defined as

$$\frac{\partial(\rho E)}{\partial t} + \frac{\partial\left(u(\rho E + p)\right)}{\partial x} = \frac{\partial}{\partial x}\left(k_{eff}\frac{\partial T}{\partial x} - \sum_j hJ + u_j(\tau)\right) + S \tag{4}$$

where $k_{eff}, J\ and\ S$ refer to the effective thermal conductivity, component diffusion flow and heat source.
The evaporation process of droplets contains the heating stage and the evaporation stage. The droplet temperature is calculated based on a heat balance relates the heat change in the droplet to the convective and latent heat transfer between the droplet and the continuous phase as follows

$$m_p c_p \frac{dT_p}{dt} = hA_p\left(T_\infty - T_p\right) - \frac{dm_p}{dt}h_{fg} + A_p\varepsilon_p\sigma\left(\theta_R^4 - T_p^4\right) \tag{5}$$

where c_p, T_p, h and T_∞ represent droplet heat capacity, droplet temperature, convective heat transfer coefficient and temperature of continuous phase, respectively. And dm_p/dt ,h_{fg} and A_p mean rate of evaporation, latent heat and the surface area of the droplet. Also, σ represents particle emissivity, ε_p stands for Stefan-Boltzmann constant, θ_R refers to radiation temperature.
T_p means droplet temperature.
The walls of the bench tube are set up as a slip boundary and the outlet boundary is set up as a pressure outlet boundary. The second-order upwind discrete equation is used, and the residual is less than 1×10^{-5} to judge the convergence of the result. The grid independence is conducted on 135 thousand, 732 thousand and 1.34 million elements on radial temperature of section 8D.
The radial height is divided by the radius of the flow field to achieve normalization, and the result is shown in Figure 5. It is found out that the temperature deviation between 732 thousand and 1.34 million elements is less than 0.6%. Thus, 732 thousand million grids are chosen for the simulation.

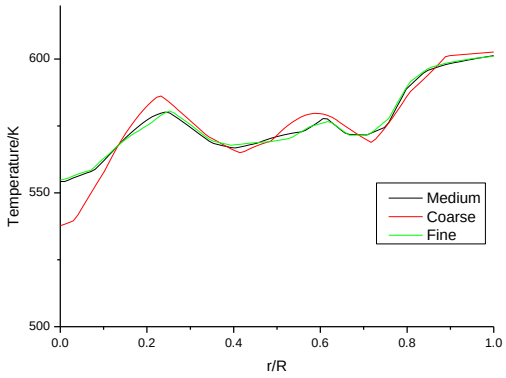

Figure 5 - Mesh independence validation

4. Results

The results mainly contain two parts. One is the waterproof effect, while the other is the consistency of the measurement results by comparison with the CFD results.

4.1 Waterproof effect

In conventional test methods, measuring points will inevitably contact with water, the primary purpose of this experiment is to check whether the probe points are in contact with water. Five heated experiments among 1%-5.5% water-air loading ratios were conducted. Whether the temperature of the measuring point is higher than the boiling point of the water under the experimental pressure (giving a 5K margin) was used as a criterion for judgment, and it turned out that under 4% water to gas loading ratio, none of the measuring points contacted with the water, while at 5% water to gas loading ratio, a measuring point in the section began to contact the water.

4.2 Consistency of the measurement results

Three sections were chosen to measure the temperature in the test. In order to verify the accuracy of the measurement method, the deviation between the measure results and the numerical results are compared. The numerical results are shown in Figure 6, which show good agreement with the results obtained by Tu Hongyan [7]. By comparison of test results with numerical results, it is found that the deviation of the section 3D is 3% at 1% water-air loading ratio, 9% at 3% water-air loading ratio, and the deviation of the section 8D is 2% at 1% water-air loading ratio, 6% at 3% water-air loading ratio. The results indicate that the test method is feasible.

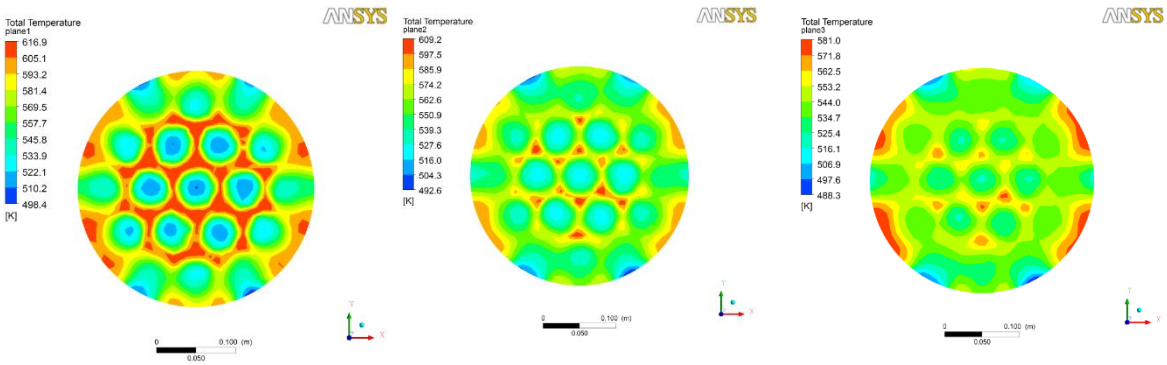

（a） section 3D （b）section 5.5D （c） section 8D

Figure 6 - Section temperature cloud diagram (at water-air loading ratio of 5.5)

Excluding the measuring points in contact with water, the deviations between the calculated average

temperature of the measuring point at the same radial height and the measured value under different test sections at corresponding water-air loading ratios are shown in Figure 7-9. Tjm is defined as the numerical average temperature of the section, and Tj is defined as the numerical temperature at the measuring point. Tc is the experiment temperature at the measuring point. It can be seen that as the distance between the probe and the nozzle increases, the deviation between the test results and the numerical results decreases. In the same section, the deviation of the measuring point is largest at 0.9R and smallest at 0.4R, while the deviation at 0.4R and 0.7R is close. For example, when the water-air loading ratio is 2%, the deviation at 0.4R measuring point in section 3D is 6%, and the deviation at 0.9R measuring point is 11%. This is because the water droplets are attached to the inner wall surface of the casing, which causes a large thermal conductivity error at measuring point. When the water-air loading ratio is 3%, the deviation is nearly 7% at 0.4R and 0.7R in the 3D section. For the test with a water to air ratio of 4% or above, the temperature deviation at the measuring point is more than 10%.

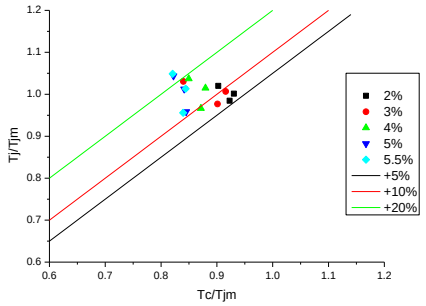

Figure 7 - Average temperature of different radial measuring points in section 3D

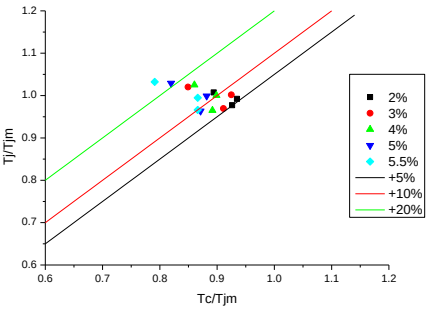

Figure 8 - Average temperature of different radial measuring points in section 5.5D

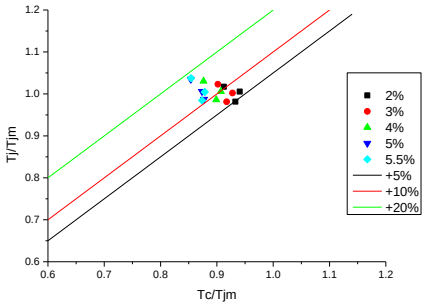

Figure 9 - Average temperature of different radial measuring points in section 8D

There are three main reasons for the deviation between the numerical results and test results. Firstly, the numerical simulation does not consider the interference of the probe in the field. Secondly, the

calibration and test method does not consider the influence of Mach number change due to the spray, which need further research. Thirdly, the probe has test errors, which include thermal conductivity, radiation, and speed errors. Considering the test conditions, the radiation error and speed error of the probe have little effect on the deviation, but the thermal conductivity error caused by droplets is drastic. The test results show that the error is small under low water-air loading ratios and large at high ratios. It also shows that the probe has a certain waterproof and heat insulation effect. However, anomalous results came out under more intense conditions. This article mainly verifies the feasibility of the test probe design and test method, and the related error analysis needs further experimental research.

5. Conclusion

The devise of a probe with corresponding calibration method used for WIPCC technique is described. The probe is proved to function well under 4% water-air loading ratio. The CFD results are consistent with the test results indicating that the probe design, calibration and test method is feasible. The test data will help to gain insights into the probe design and calibration method.

References

[1] Wilcox E C， Trout A M. Analysis of thrust augmentation of turbojet engines by water injection at compressor inlet including charts for calculating compression processes with water injection[R]. NACA-report-1006,97-116,1951.

[2] Bhargava R， Meher-Homji C B. Parametric analysis of existing gas turbines with inlet evaporative and overspray fogging[J]. *Journal of Engineering for Gas Turbines & Power,* 127(1):387-401, 2002.

[3] Daniel G，Martin C. An experimental study of water injection into a Rolls-Royce model 250-C20B turboshaft gas turbine[R]. AIAA-2008-4902.

[4] SHANG Xusheng，CAI Yuanhu，CHEN Yuchun, et al. Performance simulation of the mass injection pre-cooled TBCC engine for hypersonic vehicles[J]. *Chinese Space Science and Technology*，25(4)：54-58，2005.

[5] Sanaye S， Rezazadeh H， Aghazeynali M, et al. Effects of inlet fogging and wet compression on gas turbine performance[C] *ASME Turbo Expo 2006： Power for Land， Sea， and Air*. Barcelona, Spain：American Society of Mechanical Engineers, 769-776, 2006.

[6] Zhang H， Jiang B， Zheng Q， et al. Investigation on cooling effectiveness and flow resistance of inlet fogging location in gas turbine inlet duct[C] *ASME Turbo Expo 2015： Turbine Technical Conference and Exposition*. Montreal Canada：American Society of Mechanical Engineers：V003T20A013:1-9, 2015.

[7] Tu Hongyan, Deng Yuansong, Kang Song,etc. Numerical Simulation for Effects for Water/Air Ratio on Injection Characteristics with Water Injection Pre-Compressor Cooling[J]. *Journal of Propulsion Technology*, 38(6), 1302－1309,2017.

[8] Chaker M， Meher-Homji C B， Mee T. Inlet fogging of gas turbine engines—part I： fog droplet thermodynamics， heat transfer， and practical considerations[J]. *Journal of Engineering for Gas Turbines & Power*, 126(3):413-428, 2004.

[9] Stickney T M， Shedlov M W， Thompson D I. Total Temperature Sensors， Technical Report 5755，Revision C[R]. Rosemount Aerospace/BFGoodrich, 1-29 , 1994.

[10]Willems D E. Combustion turbine having inlet air flow temperature sensor and related methods： U.S. Patent 6，775，988[P]. 2004.

6. Copyright Statement